

# Performance of the WaveBurst algorithm on LIGO data

S Klimenko<sup>†</sup>, I Yakushin<sup>‡</sup>, M Rakhmanov<sup>†</sup> and  
G Mitselmakher<sup>†</sup>

<sup>†</sup> Department of Physics, University of Florida, Gainesville, FL 32611, USA

<sup>‡</sup> LIGO Livingston Observatory, Livingston, LA 70754, USA

**Abstract.** In this paper we describe the performance of the WaveBurst algorithm which was designed for detection of gravitational wave bursts in interferometric data. The performance of the algorithm was evaluated on the test data set collected during the second LIGO Scientific run. We have measured the false alarm rate of the algorithm as a function of the threshold and estimated its detection efficiency for simulated burst waveforms.

## 1. Introduction

A direct observation of gravitational waves (GW) produced by astrophysical sources is an ultimate goal for a new generation of detectors based on laser interferometry [1]-[4]. A broad class of expected signals are bursts which are transients of gravitational radiation with short duration, typically less than a second. They may be produced by sources such as supernova explosions, mergers of binary inspiral systems, gamma ray bursts, and other violent and energetic phenomena in the universe. The first result of burst searches with LIGO detectors has been recently reported by the LIGO collaboration [5].

At the present time the waveforms of gravitational waves from burst sources are poorly known. Consequently, burst searches employ data analysis algorithms which identify bursts with a broad range of possible waveforms. Recently several such algorithms have been developed [6, 7, 8, 9], including the algorithm called WaveBurst [10]. The WaveBurst algorithm is based on wavelet transformations and allows detection of a wide class of GW bursts by using a bank of wavelet packets [11, 12].

In this paper we describe a data analysis pipeline with a particular implementation of the WaveBurst algorithm and evaluate the pipeline performance on the data from the second LIGO Scientific run (S2). The S2 data was collected from all three LIGO detectors during a two month period beginning on February 14, 2003. We used a small fraction ( $\sim 10\%$ ) of the S2 data, which was selected as the test (playground) set for the purpose of tuning and evaluation of the burst detection algorithms. The paper is organized as follows: we begin with a brief description of the data analysis pipeline, present the measurements of the false alarm rates, and conclude with the estimation of the pipeline sensitivity.

## 2. WaveBurst data analysis pipeline

The block diagram of the WaveBurst data analysis pipeline is shown in Figure 1. The pipeline takes as input the raw time series from the GW channels of the three

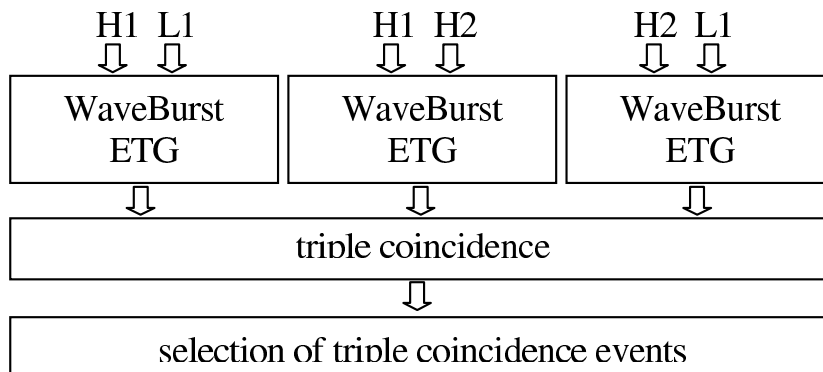


**Figure 1.** The block diagram of the WaveBurst data analysis pipeline for three LIGO detectors: H1, H2 and L1.

LIGO detectors and generates a set of potential GW burst events (triggers). The data processing stages of the pipeline are:

- production of burst triggers with the WaveBurst event trigger generator (ETG),
- reconstruction of events coincident in all three LIGO detectors,
- final selection of the triple coincidence events.

### 2.1. Production of burst triggers

The WaveBurst ETG is an implementation of the burst analysis method described in [10]. The method is based on wavelet transformations which allow time-frequency representation of data. The bursts are identified by looking for regions in the wavelet domain with an excess of power inconsistent with stationary detector noise.

The ETG takes data from the GW channels of two detectors and produces a list of coincident burst triggers. The data is processed in the following steps: 1) wavelet transformation, 2) selection of wavelet amplitudes, 3) coincidence between the channels, 4) generation of burst triggers, and 5) selection of burst triggers. During steps 1), 2) and 4) the data processing is independent for each channel. During steps 3) and 5) data from both channels is used.

The input data are time series with duration of 120 seconds and sampling rate of 8192 Hz. Using the orthogonal wavelet transformation<sup>‡</sup> the time series are converted into wavelet series  $W_{ij}$ , where  $i$  is the time index and  $j$  is the wavelet layer index. Each wavelet layer can be associated with a certain frequency band of the initial time series. Therefore, the wavelet series  $W_{ij}$  can be displayed as a time-frequency scalogram consisting of 64 wavelet layers with  $n = 15360$  pixels (data samples) each. The time-frequency resolution of the WaveBurst scalograms is the same for all wavelet layers ( $1/128$  sec  $\times$  64 Hz), which is different from dyadic time-frequency resolution of conventional wavelets [10, 13]. The constant time-frequency resolution makes the WaveBurst scalograms similar to spectrograms produced with windowed Fourier transformations.

For each layer we select a fixed fraction ( $P$ ) of pixels with largest absolute amplitudes, which are called *black pixels*. The number of black pixels is  $nP$ . All other wavelet pixels are called *white pixels*. Then we calculate rank statistics for the black pixels. The rank  $R_{ij}$  is an integer number from 1 to  $nP$  with the rank 1 assigned to the pixel with the largest amplitude. Given the rank  $R_{ij}$ , the following non-parametric statistic is computed

$$y_{ij} = -\ln\left(\frac{R_{ij}}{nP}\right). \quad (1)$$

For white pixels the value of  $y_{ij}$  is set to zero. The statistic  $y_{ij}$  has a meaning of the pixel *logarithmic significance*. Assuming Gaussian detector noise, the logarithmic significance

<sup>‡</sup> SYMLET wavelet with the filter length of 60.

can be also calculated as

$$\tilde{y}_{ij} = g_P(\tilde{w}_{ij}) = \ln(P) - \ln \left( \sqrt{2/\pi} \int_{\tilde{w}_{ij}}^{\infty} e^{-x^2/2} dx \right), \quad (2)$$

where  $\tilde{w}_{ij}$  is the absolute value of the pixel amplitude in units of the noise standard deviation. In practice, the LIGO detector noise is not Gaussian and its probability distribution function is not well known. Therefore, we use the non-parametric statistic  $y_{ij}$ , which is a more robust measure of the pixel significance than  $\tilde{y}_{ij}$ . Using the inverse function of  $g_P$  with  $y_{ij}$  as an argument, we introduce the *non-parametric amplitude*

$$w_{ij} = g_P^{-1}(y_{ij}), \quad (3)$$

and the *excess power ratio*

$$\rho_{ij} = w_{ij}^2 - 1, \quad (4)$$

which characterizes the pixel excess power above the average detector noise.

After the black pixels have been selected, we require a coincidence between the channels. Given a black pixel in the first channel, it is accepted or rejected depending on a condition applied to pixels in the corresponding time-frequency area of the second channel. The pixel is accepted if the significance of pixels in the second channel satisfies

$$y_{(i-1)j} + y_{ij} + y_{(i+1)j} > \eta, \quad (5)$$

where  $\eta$  is the *coincidence threshold*. Otherwise, the pixel is rejected. This procedure is repeated for all black pixels in the first channel. The same coincidence algorithm is applied to pixels in the second channel. As a result, a considerable number of black pixels in both channels produced by fluctuations of the detector noise is rejected. At the same time, black pixels produced by coincident bursts have a much higher acceptance probability because of the coherent excess of power in two detectors.

After the coincidence procedure is applied to both channels, the channels may have similar but not identical patterns of black pixels which form clusters. The clusters can be reconstructed separately for each channel. However, in the present WaveBurst algorithm, we merge the black pixels from both channels into one time-frequency scalogram and then run a cluster analysis. For each black pixel we define neighbors, which share a side or a vertex with the black pixel. Neighbors can be both black and white pixels. The white neighbors are called *halo* pixels. We define a cluster as a connected group of black and halo pixels. After the cluster reconstruction, we go back to the original time-frequency scalograms and calculate the cluster parameters separately for each channel. There are always two clusters, one per channel, which form a WaveBurst trigger.

The cluster parameters are calculated using black pixels only. For example, the cluster size  $k$  is defined as the number of black pixels. Other parameters, which characterize the cluster strength, are the cluster excess energy ratio  $\rho$  and the cluster *logarithmic likelihood*  $Y_k$ :

$$\rho = \sum_{i,j \in C(k)} \rho_{ij}, \quad Y_k = \sum_{i,j \in C(k)} y_{ij}, \quad (6)$$

where  $C(k)$  defines a set of black pixels in the cluster. The cluster size and the excess power ratio are used for the selection of triggers. A trigger is reported by the ETG if both clusters satisfy the conditions:  $k > 0$  and  $\rho > 6.25$ .

## 2.2. ETG tuning

There are two main ETG parameters: the black pixel fraction  $P$  and the coincidence threshold  $\eta$ . The purpose of these parameters is to control the average black pixel occupancy  $O(P, \eta)$  of the scalograms used for the cluster reconstruction. To ensure robust cluster reconstruction, the occupancy should not be greater than 1%. For white Gaussian detector noise the functional dependence  $O(P, \eta)$  can be calculated analytically. We require that  $O(P, \eta) = 0.7\%$ , which sets a constraint on  $P$  and  $\eta$ .

The selection of black pixels effectively sets a threshold on the wavelet amplitudes:  $w_{ij} > g_P^{-1}(0)$ . The larger the value of  $P$  – the lower the threshold. However, the black pixel fraction should not be greater than 31.7%, otherwise pixels with negative values of  $\rho_{ij}$  would be taken into the analysis. From the other side, with  $P$  set too small (less than a few percent), noise outliers due to instrumental glitches may consume the entire time-frequency volume available for black pixels and thus mask gravitational waves. To avoid saturation from the instrumental glitches, we run the analysis with  $P$  equal to 10%. Together with the occupancy constraint above it sets the coincidence threshold of 1.5.

For S2 playground data and selected values of  $P$  and  $\eta$ , the average trigger rate is approximately 6 Hz. Within a factor of two it is consistent with the false alarm rate expected for the white Gaussian detector noise. To reduce the ETG rates to manageable level ( $\sim 1$  Hz), we set an intermediate threshold on the cluster excess power ratio (Section 2.1) and postpone the final selection of the pipeline threshold for the post-production analysis (Section 2.4). In this case, there is no need to re-run the ETG, which is CPU and time consuming operation, for tuning of the pipeline false alarm rates and sensitivity.

## 2.3. Triple coincidence

The output of the WaveBurst ETG is a set of double coincidence triggers for a selected interferometer pair  $X \times Y$ . For three LIGO interferometers there are three possible pairs:  $L1 \times H1$ ,  $H1 \times H2$  and  $H2 \times L1$ , where  $H1$  and  $H2$  are two Hanford interferometers and  $L1$  is the Livingston interferometer. To identify triple coincidence events, we require a time-frequency coincidence of the WaveBurst triggers generated for these three pairs.

For time coincidence the following conditions are required

$$|T_{L1H1} - T_{H1H2}| < T_w, |T_{H2L1} - T_{H1H2}| < T_w, |T_{H2L1} - T_{L1H1}| < T_w, \quad (7)$$

where  $T_w$  is the time window ( $T_w = 20$  ms) and  $T_{XY}$  is the average center time of the  $X$  and  $Y$  clusters. Given the time  $t_i$  for individual pixels, the cluster center time is

calculated as

$$T = \sum_{i,j \in C(k)} t_i w_{ij}^2 / \sum_{i,j \in C(k)} w_{ij}^2. \quad (8)$$

We also apply a loose requirement on the frequency coincidence of the WaveBurst triggers. First, we calculate the minimum ( $f_{min}$ ) and maximum ( $f_{max}$ ) frequency for each interferometer pair  $X \times Y$

$$f_{min} = \min(f_{low}^X, f_{low}^Y), \quad f_{max} = \max(f_{up}^X, f_{up}^Y), \quad (9)$$

where  $f_{low}$  and  $f_{up}$  are the lower and upper frequency boundaries of the  $X$  and  $Y$  clusters. Then the trigger frequency bands are calculated as  $f_{max} - f_{min}$  for all pairs. For frequency coincidence, the bands of all three WaveBurst triggers are required to overlap.

#### 2.4. Final selection of triple coincidence events

The triple coincidence events consist of 3 WaveBurst triggers or 6 clusters. The cluster parameters are calculated separately for each interferometer, as described in Section 2.1. For the final selection of the burst triggers we use the *cluster significance*

$$Z = Y_k - \ln \left( \sum_{m=0}^{k-1} \frac{Y_k^m}{m!} \right) \quad (10)$$

derived from the logarithmic likelihood  $Y_k$  [10]. Given the significance of six clusters, we compute the *combined significance* of the triple coincidence event as

$$Z_G = \left( Z_{L1H1}^{L1} Z_{L1H1}^{H1} Z_{H2L1}^{H2} Z_{H2L1}^{L1} Z_{H1H2}^{H1} Z_{H1H2}^{H2} \right)^{1/6}, \quad (11)$$

where  $Z_{XY}^X$  ( $Z_{XY}^Y$ ) is the significance of  $X$  ( $Y$ ) cluster for the  $X \times Y$  interferometer pair. Figure 2 shows the combined significance distribution for the false alarm events found in the S2 playground data. To control the pipeline false alarm rate, we set a threshold on the value of the combined significance.

### 3. False alarm rate

Assuming there is no physical correlation between the Hanford and Livingston sites, the false alarm (FA) rate is dominated by accidental triple-coincidence events produced by fluctuations of the detector noise. For estimation of the FA rate we perform the entire WaveBurst analysis on the data with artificial time shifts between the Livingston and Hanford detectors. The false alarm triggers are generated for 46 time lags between  $-115$  and  $115$  seconds with time step of 5 seconds. The zero time lag is excluded from the analysis. Figure 3 shows the measured rates at different time lags before the final selection cut is applied to the combined significance. The measurements at different time lags are consistent with the average rate of 16.9 Hz.

As shown in Figure 4, the FA rate depends strongly on the WaveBurst combined significance cut. Without compromising much the pipeline sensitivity, the significance

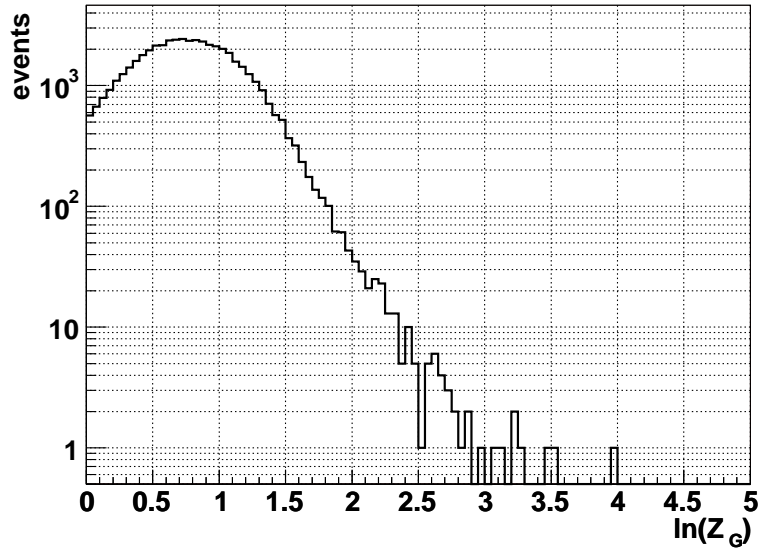


**Figure 2.** The combined significance distribution of the WaveBurst triggers produced with unphysical time lags between the Livingston and Hanford detectors.

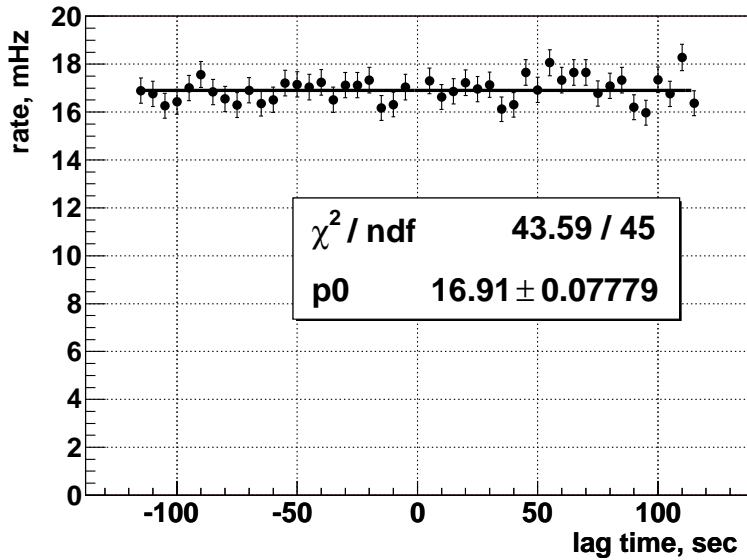


**Figure 3.** The false alarm rate before the  $Z_G$  selection cut as a function of the time lag between the Livingston and Hanford detectors.

threshold is set to 5.47 (or  $\ln(Z_G) > 1.7$ ). At this threshold the FA rate is approximately  $230 \mu\text{Hz}$  for the WaveBurst triggers in the frequency band  $64 - 4096 \text{ Hz}$ . The rate is strongly dependent on the frequency band selected for the analysis. For example, for the frequency band below  $1100 \text{ Hz}$ , the measured FA rate is approximately  $15 \mu\text{Hz}$ . Both the FA rate and the pipeline sensitivity depend on the significance threshold. Varying

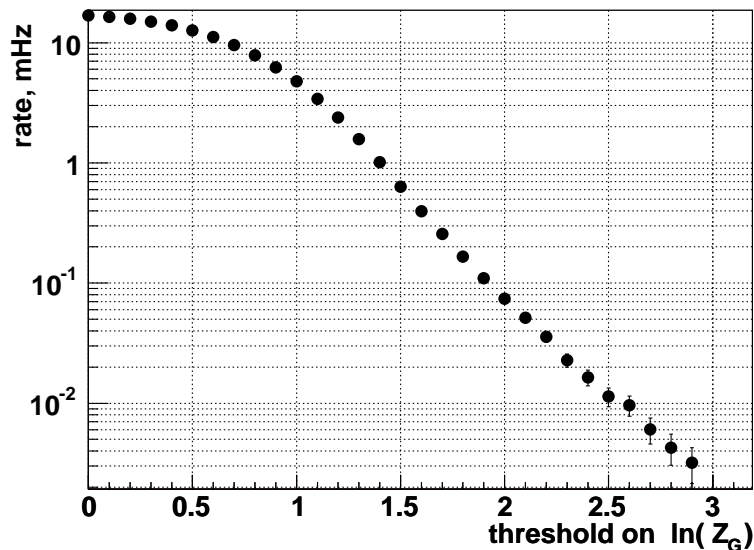


**Figure 4.** The false alarm rate as a function of the threshold on the combined significance.

the threshold, we can study the dependence of the FA rate on the sensitivity, which is an important characteristic of the pipeline. Figure 5 shows the pipeline rate as a function of the sensitivity for frequency band below 1100 Hz.

#### 4. Simulation

For estimation of the WaveBurst detection efficiency we studied the response of the analysis pipeline to simulated signals. Simulated signals with different amplitudes were injected into the GW data streams from three LIGO detectors. Then we applied the WaveBurst algorithm to find the injected signals and thus estimated the pipeline sensitivity.

Several ad-hoc and astrophysically motivated waveforms were selected for injections. These included Gaussian, sine-Gaussian waveforms and the simulated BH-BH merger waveforms described in [14]. To make the injections as realistic as possible we took into account the antenna pattern functions of the LIGO detectors and injected the waveforms at random times, accounting for the delay in the arrival time between the Hanford and Livingston sites.

##### 4.1. Simulation Procedure

A general GW burst is comprised of two waveforms  $h_+(t)$  and  $h_\times(t)$  which represent two polarizations of the gravitational wave. The signal produced at the output of the GW detector is a linear combination of these waveforms:

$$h(t) = F_+ h_+(t) + F_\times h_\times(t), \quad (12)$$

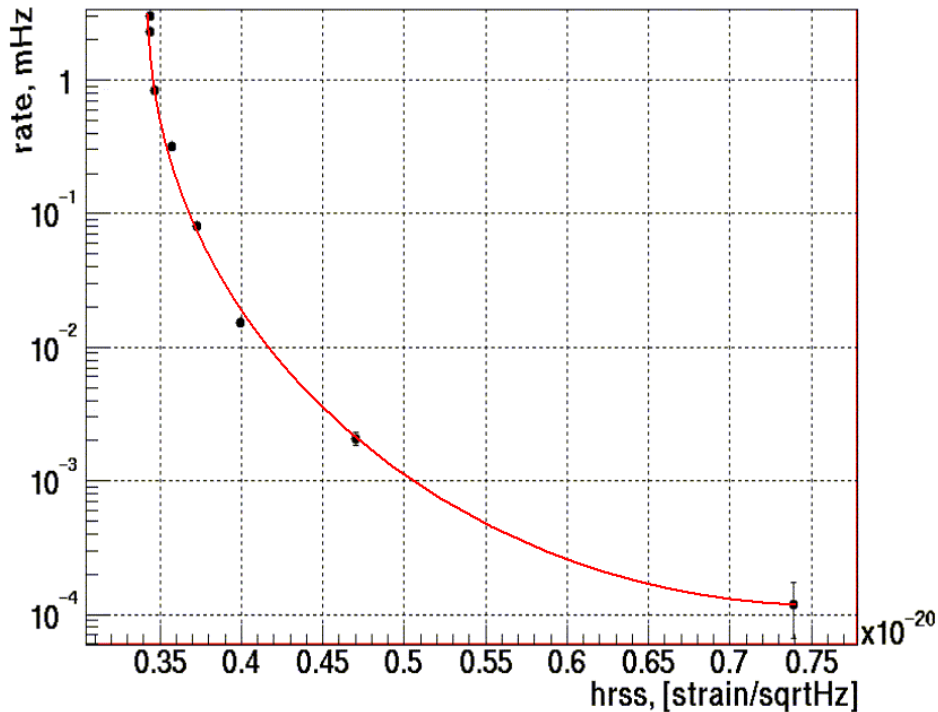


**Figure 5.** The dependence of the false alarm rate on the pipeline sensitivity for sine-Gaussian waveforms with  $f = 235$  Hz and  $Q = 9$ . Solid circles correspond to the WaveBurst triggers with  $\ln(Z_G)$  greater than 0, 0.5, 1.0, 1.25, 1.5, 1.7, 2.0, 2.5 (counting from the left). For convenience, the rate-hrss dependence is approximated with a solid line.

where  $F_+$  and  $F_\times$  are the antenna pattern functions. These functions depend on the source location in the sky (spherical angles  $\theta$  and  $\phi$ ) and its polarization angle  $\psi$ . To generate the antenna pattern functions for Hanford detectors, we explicitly construct the rotational transformation from the source coordinate frame to the Hanford frame. To obtain the  $L1$  antenna pattern we apply a second transformation – rotation from the Hanford to the Livingston detector frame.

The amplitudes of injected signals are varied to obtain the sensitivity of the algorithm as a function of the injection strength. For the Hanford data, the simulated signals are injected randomly in time at the average rate of 5 per minute. For the Livingston data, the same set of waveforms is injected with time delays, uniquely defined by the source coordinates  $\theta$  and  $\phi$ . The source coordinates are generated randomly, so the sources appear distributed uniformly on the sky (*all sky simulation*) and their polarization angles take random values between 0 and  $2\pi$ . In addition, we injected waveforms with the same strength for both sites, ignoring the antenna pattern functions. Although this simulation does not correspond to any meaningful source population, it allows us to remove the contribution of the antenna pattern functions and estimate the best pipeline sensitivity. Below we refer to this case as the *simulation with optimal orientation*.

#### 4.2. Pipeline sensitivity

The detection efficiency is a function of the injected signal strength. For a given signal strength, the detection efficiency is defined as the ratio of the number of detected waveforms to the total number of injected waveforms. We define the strength of an arbitrary burst signal as a root-sum-square strain amplitude [5]:

$$h_{\text{rss}} = \left\{ \int [h_+^2(t) + h_\times^2(t)] dt \right\}^{1/2}. \quad (13)$$

For example, the detection efficiency curve as a function of  $h_{\text{rss}}$  is shown in Figure 6 for one of the simulated signals. We determine the strength of signals detected with 50% efficiency ( $h_{50\%}$ ) and use it as a measure of the WaveBurst sensitivity. The results on the measured sensitivities are presented below for different injected waveforms and the combined significance threshold of 1.7.

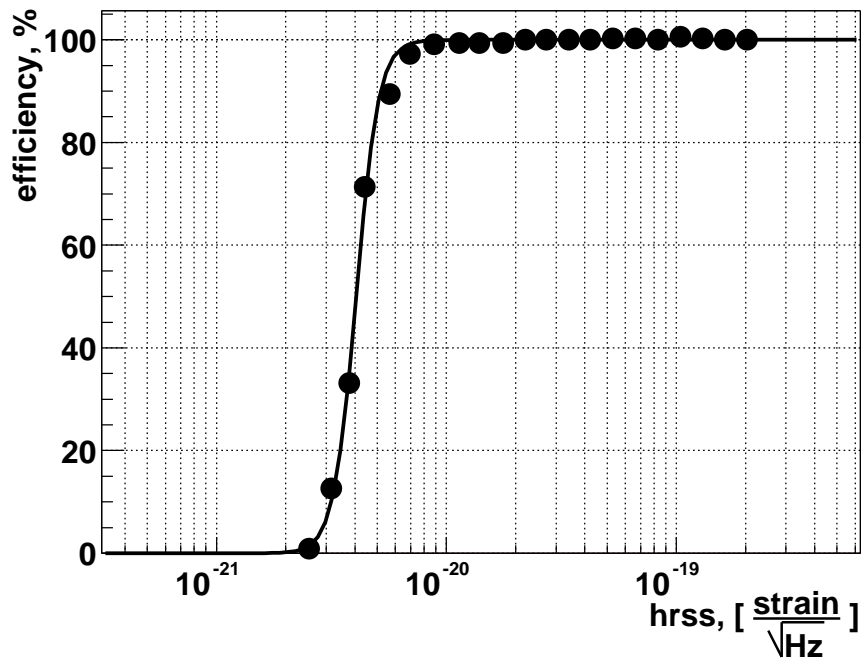


**Figure 6.** The detection efficiency for sine-Gaussian waveforms ( $f = 235$  Hz,  $Q = 9$ , optimal orientation).

The first class of injected waveforms corresponds to the GW bursts, which can be produced in the final plunge of two coalescing black holes. Both  $h_+(t)$  and  $h_\times(t)$  waveforms have been obtained by the Lazarus group [14, 15] as the result of numerical simulation of the merger and ringdown phases of a binary black hole system. These waveforms are parametrized by the total mass of the binary system in units of Solar mass  $M_\odot$ . The results on the pipeline sensitivity are summarized in Table 1.

Another class of injected waveforms is the sine-Gaussian wave [5] with the center frequency  $f$  and the quality factor  $Q = \sqrt{2}\pi f\tau$ , where  $\tau$  defines the signal duration. The results of the pipeline sensitivity to the sine-Gaussian waveforms are summarized

total mass ( $M_{\odot}$ )	10	20	30	40	50	60	70	80	90	100
sensitivity	55	24	17	14	14	15	22	32	46	58

**Table 1.** WaveBurst sensitivity (in units of  $10^{-21}$  *strain*/ $\sqrt{\text{Hz}}$ ) for black hole waveforms (all sky simulation).

in Table 2, assuming only one polarization ( $h_+$ ) of the injected signals. The sensitivity is greatest to the sine-Gaussian waveform with  $f = 235$  Hz, which lies in the frequency band with maximum detector sensitivity. Note that the pipeline has approximately the same sensitivity for two different types of sine-Gaussian waveforms:  $Q = 3$  and  $Q = 9$ .

freq. (Hz)	100	153	235	361	554	849	1304	2000
optimal								
$Q = 3$	28.2	11.5	4.8	5.5	8.2	14.0	25.4	52.2
$Q = 9$	27.3	18.8	4.0	5.1	6.7	11.5	20.3	51.2
all sky								
$Q = 3$	85.3	34.2	15.7	19.2	25.0	40.4	70.4	151.0
$Q = 9$	76.5	51.3	13.9	14.4	21.0	35.2	61.8	149.0

**Table 2.** WaveBurst sensitivity (in units of  $10^{-21}$  *strain*/ $\sqrt{\text{Hz}}$ ) for sine-Gaussian waveforms (optimal orientation and all sky simulations).

Finally, we estimated the WaveBurst sensitivity to the pure Gaussian waveforms [5], which are characterized by the duration  $\tau$  only. For these signals one polarization ( $h_+$ ) and optimal orientation are assumed. The results are summarized in Table 3.

$\tau$ (ms)	0.1	0.5	1.0	2.5	4.0
sensitivity	14.4	8.2	9.4	49.2	154.0

**Table 3.** WaveBurst sensitivity (in units of  $10^{-21}$  *strain*/ $\sqrt{\text{Hz}}$ ) for Gaussian waveforms (optimal orientation).

## 5. Conclusion

WaveBurst is a novel method for detection of gravitational wave bursts. It works in the wavelet domain and allows detection of a wide class of GW bursts by using a large bank of wavelet packets. Using the S2 LIGO playground data we evaluated the performance of the WaveBurst data analysis pipeline. The pipeline sensitivity is limited by thresholds on: the wavelet amplitudes (defined by the ETG parameters  $P$  and  $\eta$ ), the cluster excess power ratio, and the combined significance of the triple coincidence events. The maximum pipeline sensitivity is approximately  $4 \times 10^{-21}$  *strain*/ $\sqrt{\text{Hz}}$  for

sine-Gaussian signals corresponding to optimal orientation of sources with respect to the LIGO detectors. Averaged over the entire sky, the pipeline strain sensitivity becomes  $14 \times 10^{-21} \text{ strain}/\sqrt{\text{Hz}}$ . The false alarm rate of the pipeline is dominated by accidental triple coincidence events produced by fluctuations in the detector noise. Using time shift analysis we estimated the WaveBurst false alarm rate as a function of the combined significance threshold. For the threshold of 1.7, the false alarm rates are  $15 \mu\text{Hz}$  and  $230 \mu\text{Hz}$  for frequency bands below 1100 Hz and 4096 Hz respectively. Thus we have shown that the WaveBurst algorithm has low false alarm rates and high sensitivity to simulated burst waveforms.

## Acknowledgments

We thank Peter Saulson for comments on the paper. We also thank the LIGO laboratory and the LIGO Scientific Collaboration which enabled this work by constructing and operating the LIGO interferometers. We gratefully acknowledge the support of the United States National Science Foundation for the construction and operation of the LIGO Laboratory and the Particle Physics and Astronomy Research Council of the United Kingdom, the Max-Planck-Society and the State of Niedersachsen/Germany for support of the construction and operation of the GEO600 detector. We also gratefully acknowledge the support of the research by these agencies and by the Australian Research Council, the Natural Sciences and Engineering Research Council of Canada, the Council of Scientific and Industrial Research of India, the Department of Science and Technology of India, the Spanish Ministerio de Ciencia y Tecnologia, the John Simon Guggenheim Foundation, the David and Lucile Packard Foundation, the Research Corporation, and the Alfred P. Sloan Foundation. This work is also supported by the US National Science Foundation grants PHY-0244902 and PHY-0070854. The paper has been assigned the LIGO Laboratory document number LIGO-P040012-00-Z.

## References

- [1] Abbott B *et al* 2004 *Nucl. Instrum. Methods* **517** 154
- [2] Willke B *et al* 2002 *Class. Quantum Grav.* **19** 1377
- [3] Acernese F *et al* 2002 *Class. Quantum Grav.* **19** 1421
- [4] Tagoshi H *et al* 2001 *Phys. Rev. D* **63** 062001
- [5] Abbott B *et al* 2004 *Phys. Rev. D* **69** 102001
- [6] Anderson W and Balasubramanian R 1999 *Phys. Rev. D* **60** 102001
- [7] Mohanty S 2000 *Phys. Rev. D* **61** 122002
- [8] Anderson W, Brady P, Creighton J and Flanagan E 2001 *Phys. Rev. D* **63** 042003
- [9] Sylvestre J 2002 *Phys. Rev. D* **66** 102004
- [10] Klimenko S and Mitselmakher G 2004 *A wavelet method for detection of gravitational wave bursts* (in this volume)
- [11] Vidakovic B 1999 *Statistical modeling by wavelets* (New York: Wiley Interscience)
- [12] Coifman R, Meyer Y and Wickerhauser M 1992 *Wavelet analysis and signal processing* In Ruskai M *et al* *Wavelets and their applications* pages 153-178 (Jones and Bartlett Publishers, Sudbury, MA)

- [13] Daubechies I 1992 *Ten lectures on wavelets* (Philadelphia: SIAM)
- [14] Baker J, Companelli M and Lousto C 2002 *Phys. Rev. D* **65** 044001
- [15] Baker J, Companelli M, Lousto C and Takahashi R 2002 *Phys. Rev. D* **65** 124012